

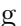



































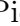









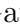







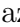


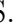

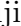










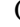




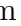
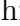
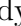




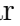
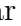
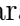



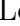
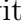









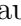

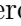
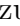
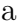


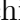




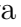




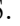
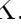





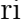

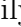



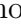

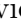






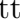

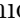










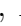







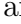



Observation of charmed strange meson pair production in $\Upsilon(2S)$ decays and in e^+e^- annihilation at $\sqrt{s} = 10.52$ GeV

B. S. Gao , W. J. Zhu , X. L. Wang , I. Adachi , H. Aihara , D. M. Asner ,
V. Aulchenko , T. Aushev , R. Ayad , V. Babu , Sw. Banerjee , M. Bauer ,
P. Behera , K. Belous , J. Bennett , M. Bessner , V. Bhardwaj , T. Bilka ,
D. Biswas , A. Bobrov , D. Bodrov , A. Bondar , A. Bozek , M. Bračko ,
P. Branchini , T. E. Browder , A. Budano , D. Červenkov , M.-C. Chang ,
P. Chang , V. Chekelian , B. G. Cheon , K. Chilikin , H. E. Cho , K. Cho ,
S.-K. Choi , Y. Choi , S. Choudhury , D. Cinabro , G. De Nardo , G. De Pietro ,
R. Dhamija , F. Di Capua , J. Dingfelder , Z. Doležal , T. V. Dong , P. Ecker ,
T. Ferber , D. Ferlewicz , B. G. Fulsom , V. Gaur , A. Giri , E. Graziani ,
T. Gu , K. Gudkova , C. Hadjivasiliou , K. Hayasaka , H. Hayashii , S. Hazra ,
M. T. Hedges , D. Herrmann , W.-S. Hou , C.-L. Hsu , T. Iijima , K. Inami ,
N. Ipsita , A. Ishikawa , R. Itoh , M. Iwasaki , W. W. Jacobs , E.-J. Jang ,
S. Jia , Y. Jin , K. K. Joo , T. Kawasaki , C. Kiesling , C. H. Kim ,
D. Y. Kim , K.-H. Kim , Y.-K. Kim , K. Kinoshita , P. Kodyš , T. Konno ,
A. Korobov , S. Korpar , P. Križan , M. Kumar , R. Kumar , K. Kumara ,
A. Kuzmin , Y.-J. Kwon , Y.-T. Lai , S. C. Lee , D. Levit , P. Lewis ,
L. K. Li , L. Li Gioi , J. Libby , K. Lieret , D. Liventsev , Y. Ma ,
M. Masuda , T. Matsuda , S. K. Maurya , F. Meier , M. Merola , R. Mizuk ,
I. Nakamura , M. Nakao , D. Narwal , A. Natchii , L. Nayak , M. Niiyama ,
N. K. Nisar , S. Nishida , S. Ogawa , P. Pakhlov , G. Pakhlova , S. Pardi ,
J. Park , S. Patra , S. Paul , T. K. Pedlar , R. Pestotnik , L. E. Piilonen ,
T. Podobnik , E. Prencipe , M. T. Prim , G. Russo , S. Sandilya , V. Savinov ,
G. Schnell , C. Schwanda , Y. Seino , K. Senyo , M. E. Sevier , W. Shan ,
C. Sharma , J.-G. Shiu , B. Shwartz , E. Solovieva , M. Starič , Z. S. Stottler ,
M. Sumihama , K. Tanida , F. Tenchini , M. Uchida , T. Uglov , Y. Unno ,
S. Uno , S. E. Vahsen , K. E. Varvell , D. Wang , E. Wang , M.-Z. Wang ,
S. Watanuki , E. Won , X. Xu , B. D. Yabsley , W. Yan , S. B. Yang ,
J. H. Yin , Y. Yook , C. Z. Yuan , L. Yuan , V. Zhilich , and V. Zhukova 

(The Belle Collaboration)

(Dated: August 23, 2023)

Abstract

We observe the process $\Upsilon(2S) \rightarrow D_s^{(*)+} D_{sJ}^-$ and continuum production $e^+e^- \rightarrow D_s^{(*)+} D_{sJ}^-$ at $\sqrt{s} = 10.52$ GeV (and their charge conjugates) using the data samples collected by the Belle detector at KEKB, where D_{sJ}^- is $D_{s1}(2536)^-$ or $D_{s2}^*(2573)^-$. Both D_{sJ}^- states are identified through their decay into $\bar{K}\bar{D}^{(*)}$. We measure the products of branching fractions $\mathcal{B}(\Upsilon(2S) \rightarrow D_s^{(*)+} D_{sJ}^-) \mathcal{B}(D_{sJ}^- \rightarrow \bar{K}\bar{D}^{(*)})$ and the Born cross sections $\sigma^{\text{Born}}(e^+e^- \rightarrow D_s^{(*)+} D_{sJ}^-) \mathcal{B}(D_{sJ}^- \rightarrow \bar{K}\bar{D}^{(*)})$, and then compare the ratios $R_1 \equiv \mathcal{B}(\Upsilon(2S) \rightarrow D_s^{(*)+} D_{sJ}^-) / \mathcal{B}(\Upsilon(2S) \rightarrow \mu^+\mu^-)$ for $\Upsilon(2S)$ decays and $R_2 \equiv \sigma^{\text{Born}}(e^+e^- \rightarrow D_s^{(*)+} D_{sJ}^-) / \sigma^{\text{Born}}(e^+e^- \rightarrow \mu^+\mu^-)$ for continuum production. We obtain $R_1/R_2 = 9.7 \pm 2.3 \pm 1.1$, $6.8 \pm 2.1 \pm 0.8$, $10.2 \pm 3.3 \pm 2.5$, and $3.4 \pm 2.1 \pm 0.5$ for the $D_s^+ D_{s1}(2536)^-$, $D_s^{*+} D_{s1}(2536)^-$, $D_s^+ D_{s2}^*(2573)^-$, and $D_s^{*+} D_{s2}^*(2573)^-$ final states in the $D_{sJ}^- \rightarrow K^- \bar{D}^{(*)0}$ modes, respectively. Therefore, the strong decay is expected to dominate in the $\Upsilon(2S) \rightarrow D_s^{(*)+} D_{sJ}^-$ processes. We also measure the ratios of branching fractions $\mathcal{B}(D_{s1}(2536)^- \rightarrow K_S^0 D^{*}(2010)^-) / \mathcal{B}(D_{s1}(2536)^- \rightarrow K^- D^{*}(2007)^0) = 0.48 \pm 0.07 \pm 0.02$ and $\mathcal{B}(D_{s2}^*(2573)^- \rightarrow K_S^0 D^-) / \mathcal{B}(D_{s2}^*(2573)^- \rightarrow K^- D^0) = 0.49 \pm 0.10 \pm 0.02$, which are consistent with isospin symmetry. The second ratio is the first measurement of this quantity. Here, the first uncertainties are statistical and the second are systematic.

PACS numbers: 14.40.Gx, 13.25.Gv, 13.66.Bc

I. INTRODUCTION

Much of the plethora of new quarkonium states observed in the last decades has been studied at electron-positron colliders [1]. These accelerators have collected large data samples at center of mass (c.m.) energies (\sqrt{s}) corresponding to both the vector charmonium and the vector bottomonium states, which are produced copiously due to resonance enhancements in the cross sections. A vector quarkonium state decays either electromagnetically through the annihilation process into a virtual photon or into three gluons mediated by the strong interaction. We can thereby separate the dynamics of electromagnetic and strong charmed meson production through complementary measurements at energies above or below the quarkonium state, which are called “off-resonance.” Here, only quantum electrodynamics (QED) processes contribute and thus allow measurements free from hadronic structure effects and quantum chromodynamics (QCD) related process present for heavy quarkonia.

At \sqrt{s} significantly above the production threshold and far from quarkonium resonances, the production rates of $e^+e^- \rightarrow q\bar{q}$ are approximately proportional to the quark charge squared, so that $e^+e^- \rightarrow c\bar{c}$ is about 40% of the total hadronic production at $\sqrt{s} = 10.52$ GeV (60 MeV below the $\Upsilon(4S)$). This provides an opportunity to study the charmed hadrons, including charmed mesons, charmed strange mesons, and charmed baryons. However, this kind of study was rarely done before. This is also true for the OZI suppressed hadronic decays of the narrow $\Upsilon(nS)$ states; hundreds of millions of $\Upsilon(nS)$ events have been accumulated at Belle and BaBar, but such studies are scarce. The open charm content of bottomonium hadronic decays can be used as a tool to probe the post- $b\bar{b}$ -annihilation fragmentation processes [2]. Within the QCD approach, the charm quarks are expected to be produced in $\Upsilon(nS)$ decay only by a process in which a virtual timelike gluon of large invariant mass is produced in the initial decay process, and subsequently decays into a pair of charmed hadrons [3]. Using a data sample of $(98.6 \pm 0.9) \times 10^6$ $\Upsilon(2S)$ events, BaBar

measures $\mathcal{B}[\Upsilon(1S) \rightarrow D^{*+}X] = (2.52 \pm 0.13 \pm 0.15)\%$ [4], which is considerable in excess of that expected from $b\bar{b}$ annihilation into a single photon. This excess is seen to be in agreement with a prediction based on splitting a virtual photon [5], but appear to be too small to accommodate an octet-state contribution [6]. Here and hereinafter, the first uncertainty quoted is statistical while the second corresponds to the total systematic uncertainty. However, no more measurement on the charm hadron in $\Upsilon(nS)$ decays can be found [7]. It is argued that the suppression of charm production on the $\Upsilon(nS)$ resonance is at least consistent with the analogous case of strangeness production on ψ and $\psi(2S)$, and it would be quite instructive to study the topology of such events where charm is actually produced [8].

Here, we present searches for $D_s^{(*)+}D_{sJ}^-$ with the subsequent decay $D_{sJ}^- \rightarrow \bar{K} + \bar{D}^{(*)}$ in $\Upsilon(2S)$ decays and in continuum e^+e^- annihilation, using data recorded with the Belle detector operated at the KEKB asymmetric-energy e^+e^- collider [9]. Charge-conjugated modes are implicitly included throughout the paper. For the $\Upsilon(2S)$ data sample, we have collected data corresponding to an integrated luminosity of 24.7 fb^{-1} at a c.m. energy corresponding to the $\Upsilon(2S)$ resonance. We determine the number of produced $\Upsilon(2S)$ events to be $(158 \pm 4) \times 10^6$ using inclusive hadronic decays. The continuum production of the various final states is based on an off-resonance data sample collected using an integrated luminosity of 89.5 fb^{-1} at $\sqrt{s} = 10.52 \text{ GeV}$. We use these two data samples to separate the dynamics of electromagnetic and strong charmed hadron production at the off-resonance energy and the $\Upsilon(2S)$ peak.

We only include the following D_{sJ}^- states, which are both established and emit a kaon in their decay: $D_{s1}(2536)^-$ and $D_{s2}^*(2573)^-$; the kaon can be either charged or neutral (K_S^0). We use the technique of partial reconstruction for the D_{sJ}^- final state: the final state is tagged through the full reconstruction of the $D_s^{(*)+}$, and the recoiling D_{sJ}^- is tagged by a kaon produced in the decay $D_{sJ}^- \rightarrow \bar{K} + \bar{D}^{(*)}$. The remaining $\bar{D}^{(*)}$ is observed indirectly through its recoil against the $D_s^{(*)+} - \bar{K}$ system using the known kinematics of the initial state. This circumvents the problem of low efficiencies for the reconstruction of D mesons associated with the large variety of possible decay processes.

II. THE BELLE DETECTOR AND MONTE CARLO SIMULATION

The Belle detector is a large-solid-angle magnetic spectrometer [10] using a silicon vertex detector, a 50-layer central drift chamber, an array of aerogel threshold Cherenkov counters, a barrel-like arrangement of time-of-flight scintillation counters, and an electromagnetic calorimeter (ECL) comprised of CsI(Tl) crystals located inside a super-conducting solenoid coil that provides a 1.5 T magnetic field. An iron flux return located outside of the coil is instrumented to detect K_L^0 mesons and to identify muons. The origin of the coordinate system is defined as the position of the nominal interaction point. In the cylindrical coordinates, the z axis is aligned with the direction opposite the e^+ beam and points along the magnetic field within the solenoid, and r is the radial distance.

We simulate the full chain $\Upsilon(2S)/e^+e^- \rightarrow D_s^{(*)+}D_{sJ}^-$, in which D_{sJ}^- is $D_{s1}(2536)^-$ or $D_{s2}^*(2573)^-$, using the EvtGen generator [11]. We simulate the angular distributions of $D_s^{(*)+}D_{sJ}^-$ according to the J^P quantum numbers of $D_s^{(*)+}$ and D_{sJ}^- . Here, we take $J^P = 1^-$ for D_s^{*+} according to the recent BESIII measurement [12]. Four decay modes of D_{sJ}^- are simulated: $K^- + \bar{D}^0$, $K_S^0 + D^-$, $K^- + \bar{D}^*(2007)^0$, and $K_S^0 + D^*(2010)^-$. Again, the D mesons (\bar{D}^0 , D^- , $\bar{D}^*(2007)^0$, and $D^*(2010)^-$) are not reconstructed, but determined in the recoil of the $D_s^{(*)+}$ and the kaon from the D_{sJ}^- decay, so that the decays of D mesons are inclusive.

We simulate the response of the Belle detector using a GEANT3-based Monte Carlo (MC) technique [13].

III. EVENT SELECTION CRITERIA AND RECONSTRUCTION

We search for the tagging D_s^+ using six final states: $\phi\pi^+$, $K_S^0 K^+$, $\bar{K}^*(892)^0 K^+$, $\rho^+ \phi$, $\eta\pi^+$ and $\eta'\pi^+$. The decay of D_s^{*+} only proceeds through $D_s^{*+} \rightarrow D_s^+ \gamma$.

We reconstruct $D_s^{(*)+} D_{sJ}^-$ final states by first selecting well-measured charged tracks and photon candidates. A well-measured charged track has an impact parameter $dr < 1.5$ cm in the $r - \phi$ plane with respect to the interaction point and a displacement $|dz| < 5$ cm in the $r - z$ plane. We require a transverse momentum larger than 0.1 GeV/c. We identify each charged track by combining the information from different detector subsystems and form the likelihood \mathcal{L}_i [14] for each particle species i , denoting π or K . Tracks with $\mathcal{R}_K = \frac{\mathcal{L}_K}{\mathcal{L}_K + \mathcal{L}_\pi} > 0.6$ are treated as kaons, while those with $\mathcal{R}_K < 0.4$ are assumed to be pions. The identification efficiency is about 95% for both K and π . Photons are identified through a cluster in the ECL, which does not align with any charged track.

We reconstruct the K_S^0 , ϕ , $\bar{K}^*(892)^0$, and ρ^+ candidates in their respective decay channels into $\pi^+ \pi^-$, $K^+ K^-$, $K^- \pi^+$, and $\pi^+ \pi^0$. For candidate K_S^0 mesons, we use pairs of oppositely charged particles that originate from a common vertex and assign the pion-mass hypothesis. We use a multivariate technique to improve the purity of the K_S^0 candidate sample by rejecting combinatorial background [15], which we identify with neural network (NN) [16] based algorithms. For the invariant mass ($M_{\pi^+ \pi^-}$) of $\pi^+ \pi^-$ pairs we obtain a resolution of $\sigma \approx 5$ MeV/ c^2 , and we define the signal region for K_S^0 by $|M_{\pi^+ \pi^-} - m_{K_S^0}| < 3\sigma$. Here, $m_{K_S^0}$ is the nominal mass of the K_S^0 [7]. Correspondingly, we choose the range of all signal mass windows to have $\Delta m = \pm 3\sigma$ around their respective nominal masses [7], unless stated otherwise. The corresponding resolution for the invariant mass of $K^+ K^-$ pairs, $M_{K^+ K^-}$, is $\sigma \approx 3.3$ MeV/ c^2 . The $\bar{K}^*(892)^0$ meson has a natural width of 47.3 MeV, which is much larger than the experimental resolution for $K^- \pi^+$ pairs. We define the $\bar{K}^*(892)^0$ signal region to be $|M_{K^- \pi^+} - m_{\bar{K}^*(892)^0}| < 105$ MeV/ c^2 , where $M_{K^- \pi^+}$ is the invariant mass of $K^- \pi^+$ and $m_{\bar{K}^*(892)^0}$ is the nominal mass of $\bar{K}^*(892)^0$ [7]. Since the width of the ρ^+ of about 150 MeV is dominated by the natural width, the signal region is selected by $|M_{\pi^+ \pi^0} - m_{\rho^+}| < 200$ MeV/ c^2 , in which $M_{\pi^+ \pi^0}$ is the invariant mass of $\pi^+ \pi^0$ and m_{ρ^+} is the nominal mass of ρ^+ [7].

We combine pairs of photons to form π^0 candidates. For this, we require the energies of photons (E_γ) from π^0 decays to exceed $E_\gamma > 25$ MeV in the barrel ($32.2^\circ < \theta < 128.7^\circ$) and $E_\gamma > 50$ MeV in the endcaps ($12.0^\circ < \theta < 31.4^\circ$ or $131.5^\circ < \theta < 157.1^\circ$) of the ECL, with the polar angles specified in the laboratory frame. The two-photon mass resolution for $M_{\gamma\gamma}$ is $\sigma \approx 5$ MeV/ c^2 . We reconstruct η mesons from their decay into both $\pi^+ \pi^- \pi^0$ and $\gamma\gamma$. In the $\gamma\gamma$ mode, we require $E_\gamma > 150$ MeV. The corresponding mass resolution for $M_{\pi^+ \pi^- \pi^0}$ is $\sigma \approx 4$ MeV/ c^2 and for $M_{\gamma\gamma}$ the resolution is $\sigma \approx 13.5$ MeV/ c^2 . For the selection of η' candidates, we use a combination of η and $\pi^+ \pi^-$ pairs. The invariant mass resolution for $\eta\pi^+ \pi^-$ is $\sigma_{\eta\pi^+ \pi^-} \approx 5$ MeV/ c^2 .

In Fig. 1(a) and (c), we show the combined distribution $M_{h_1 h_2}$ of $M_{\phi\pi^+}$, $M_{K_S^0 K^+}$, $M_{\bar{K}^*(892)^0 K^+}$, $M_{\rho^+ \phi}$, $M_{\eta\pi^+}$ and $M_{\eta'\pi^+}$ from the $\Upsilon(2S)$ data sample (upper row) and the continuum data sample (lower row). We do not apply a mass constraint for π^0 , η or η' . Instead, we take the advantage of the mass difference. Taking the $D_s^+ \rightarrow \eta\pi^+$ with $\eta \rightarrow \gamma\gamma$

as an example, we use $M_{\eta\pi^+} = M_{\gamma\gamma\pi^+} - M_{\gamma\gamma} + m_\eta$, where the invariant mass $M_{\gamma\gamma\pi^+}$ ($M_{\gamma\gamma}$) is calculated from the sum of the 4-momenta of $\gamma\gamma\pi^+$ ($\gamma\gamma$). In this way, the mass resolution of the D_s^+ signal in $M_{\eta\pi^+}$ is improved from 19.7 MeV/ c^2 to 13.0 MeV/ c^2 according to signal MC simulation. We fit the D_s^+ signal in $M_{h_1h_2}$ with a Gaussian function and describe the background through a second-order polynomial function. We obtain a mass resolution of $\sigma_{D_s^+} = 6.7 \pm 0.1$ MeV/ c^2 in data, which is used to define the signal region for D_s^+ , while the corresponding resolution is 6.5 MeV/ c^2 in signal MC simulations. Besides the D_s^+ signal, we also define sideband regions through $|M_{h_1h_2} - m_{D_s^+} \pm 9\sigma_{D_s^+}| < 3\sigma_{D_s^+}$. Since the fraction of multi-combination in D_s^+ reconstruction is only about 3%, we allow multiple candidates of D_s^+ in one event.

We reconstruct D_s^{*+} candidates from the above D_s^+ sample using the γD_s^+ final state. For this, we require the photon energy to exceed $E_\gamma > 50$ MeV in the barrel and $E_\gamma > 100$ MeV in the endcaps of the ECL. The corresponding invariant mass distributions $M_{\gamma D_s^+}$ for γD_s^+ from the $\Upsilon(2S)$ and continuum data samples are shown in Fig. 1(b) and (d). Here, we use $M_{\gamma D_s^+} = M_{\gamma h_1h_2} - M_{h_1h_2} + m_{D_s^+}$, where the invariant mass $M_{\gamma h_1h_2}$ is calculated from the sum of the 4-momenta of γh_1h_2 . We fit to the $M_{\gamma D_s^+}$ distribution between 2.07 GeV/ c^2 and 2.15 GeV/ c^2 using two Gaussian functions for the D_s^{*+} signal and a second order polynomial function for the background. We use $\sigma \equiv \sqrt{f_1 \times (\sigma_1^2 + m_1^2) + f_2 \times (\sigma_2^2 + m_2^2) - m^2}$ with $m = f_1 \times m_1 + f_2 \times m_2$ to define the mass resolution of the D_s^{*+} signals, where m_1 (m_2), σ_1 (σ_2) and f_1 (f_2) are the mean, the standard deviation and the fraction of the first (second) Gaussian function. We obtain the mass resolution of $\sigma_{D_s^{*+}} = 6.7 \pm 0.4$ MeV/ c^2 in data and 7.0 MeV/ c^2 in signal MC simulations, which agree well with each other. Again, in addition to the signal region for D_s^{*+} , we define sideband regions through $|M_{\gamma D_s^+} - m_{D_s^{*+}} \pm 9\sigma_{D_s^{*+}}| < 3\sigma_{D_s^{*+}}$. As we aim to study the $D_s^{*+}\bar{K}$ recoil spectrum, we apply mass-constrained fits to the D_s^{*+} candidates in the signal region to improve their momentum resolution. We find that 35% of the events have multiple D_s^{*+} candidates. In these cases, we select the candidate with the minimum χ^2 from the mass-constraint fit. For the candidates in each D_s^{*+} mass sideband, we apply the mass constraint to the center of the sideband and select the combination with minimum χ^2 as well. To estimate the size of the peaking component in the selected D_s^{*+} sample due to the minimum χ^2 requirement, we apply the same mass constraints to events in the D_s^+ sidebands. As shown in Fig. 1(b) and (d), the D_s^+ mass sideband events can describe the peaks in the D_s^{*+} mass sidebands, and therefore can be used to estimate the peaking component in the D_s^{*+} mass signal region reliably. Events with $|M_{\gamma D_s^+} - m_{D_s^{*+}}| < 50$ MeV/ c^2 are removed for the $D_s^+ D_{sJ}^-$ search.

The search for $\bar{D}^{(*)}$ requires a \bar{K} meson reconstructed in addition to $D_s^{(*)+}$. We determine the $\bar{D}^{(*)}$ signal through the recoil of $D_s^{(*)+}\bar{K}$ using the calculated mass:

$$M_{\bar{D}^{(*)}} = M_{D_s^{(*)+}\bar{K}}^{\text{recoil}} \equiv \sqrt{(E_{\text{c.m.}} - E_{D_s^{(*)+}} - E_{\bar{K}})^2 - (\vec{p}_{\text{c.m.}} - \vec{p}_{D_s^{(*)+}} - \vec{p}_{\bar{K}})^2}, \quad (1)$$

and isolate the possible production of D_{sJ}^- states in the $\bar{K}\bar{D}^{(*)}$ final states through their recoil using the following equation:

$$M_{\bar{K}\bar{D}^{(*)}} = M_{D_s^{(*)+}\bar{K}}^{\text{recoil}} \equiv \sqrt{(E_{\text{c.m.}} - E_{D_s^{(*)+}})^2 - (\vec{p}_{\text{c.m.}} - \vec{p}_{D_s^{(*)+}})^2}. \quad (2)$$

Here, $E_{\text{c.m.}}$ and $\vec{p}_{\text{c.m.}}$ are the energy and 3-momentum of e^+e^- in the collision system, $E_{D_s^{(*)+}}$ ($E_{\bar{K}}$) and $\vec{p}_{D_s^{(*)+}}$ ($\vec{p}_{\bar{K}}$) are those of $D_s^{(*)+}$ (\bar{K}), respectively. We show the $M_{D_s^{(*)+}\bar{K}}^{\text{recoil}}$ distributions

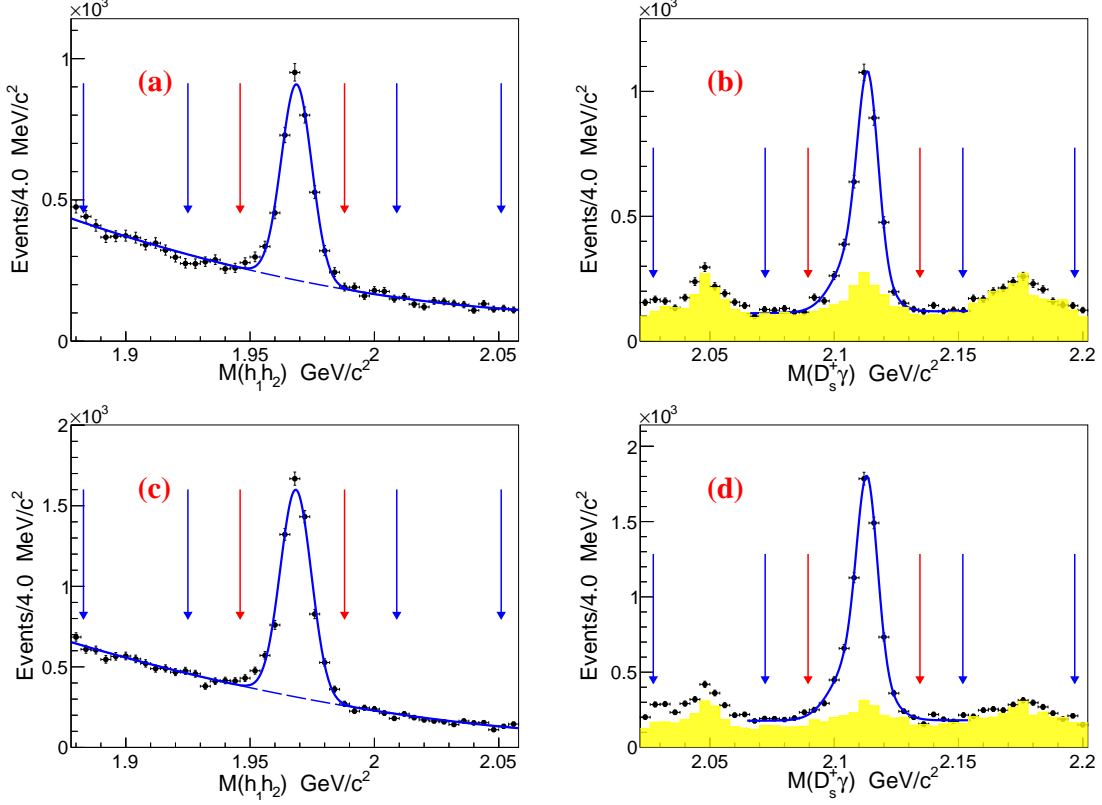


FIG. 1. Invariant mass distributions of (a,c) the combinations of $\phi\pi^+$, $K_S^0 K^+$, $\bar{K}^*(892)^0 K^+$, $\rho^+ \phi$, $\eta\pi^+$, and $\eta'\pi^+$ for D_s^+ candidates and (b,d) the combinations of γD_s^+ for $D_s^{(*)+}$ candidates in $\Upsilon(2S)$ data sample (upper panels) and continuum data sample (lower panels). The red arrows show the signal region of D_s^+ or $D_s^{(*)+}$ and the blue arrows show the related sideband regions. The shaded histogram in (b) and (d) shows backgrounds estimated from D_s^+ mass sidebands. The curves show the best fit results using Gaussian functions for the D_s^+ and $D_s^{(*)+}$ signals, respectively.

versus $M_{D_s^{(*)+}}^{\text{recoil}}$ from the two data samples in Fig. 2(a) and (b), and the signal MC simulations of $\Upsilon(2S)$ decays and continuum productions in Fig. 2(c) and (d). There are clear bands in the distributions of data corresponding to the production of the $D_{s1}(2536)^-$ signal in the $\bar{D}^* \bar{K}$ ($\bar{D}^*(2007)^0 K^-$ or $D^*(2010)^- K_S^0$) final state and $D_{s2}^-(2573)$ signal in the $\bar{D} \bar{K}$ ($\bar{D}^0 K^-$ or $D^- K_S^0$) final state, and they agree well with the signal MC simulations. The mass resolutions of $M_{D_s^{(*)+} \bar{K}}^{\text{recoil}}$ and $M_{D_s^{(*)+}}^{\text{recoil}}$ are large due to the common variables $E_{D_s^{(*)+}}$ and $\vec{p}_{D_s^{(*)+}}$ in Eqs. (1) and (2). The mass resolution of \bar{D} from the decay of D_{sJ}^- in $M_{D_s^{(*)+} \bar{K}}^{\text{recoil}}$ is about 50 MeV/c², and the signal region is defined to be $|M_{D_s^{(*)+} \bar{K}}^{\text{recoil}} - m_{\bar{D}}| < 150$ MeV/c². We fit to the \bar{D}^* mass distribution with two Gaussian functions, and obtain the narrower one with a mass resolution of 31.8 ± 0.3 MeV/c² and a signal fraction of about 34% and the wider one with a mass resolution of 74.2 ± 1.0 MeV/c² and a signal fraction of about 66%. We define the signal region to be $|M_{D_s^{(*)+} \bar{K}}^{\text{recoil}} - m_{\bar{D}^*}| < 200$ MeV/c², which has a selection efficiency of about 95%. Here, $m_{\bar{D}}$ is the nominal mass of \bar{D}^0 or D^- , and $m_{\bar{D}^*}$ is the nominal mass of the $\bar{D}^*(2007)^0$ or $D^*(2010)^-$ [7]. With the events in the D_s^+ or $D_s^{(*)+}$ mass sidebands, no peaking background is found for the $\bar{D}^{(*)}$ signal in the $M_{D_s^{(*)+} \bar{K}}^{\text{recoil}}$ distributions.

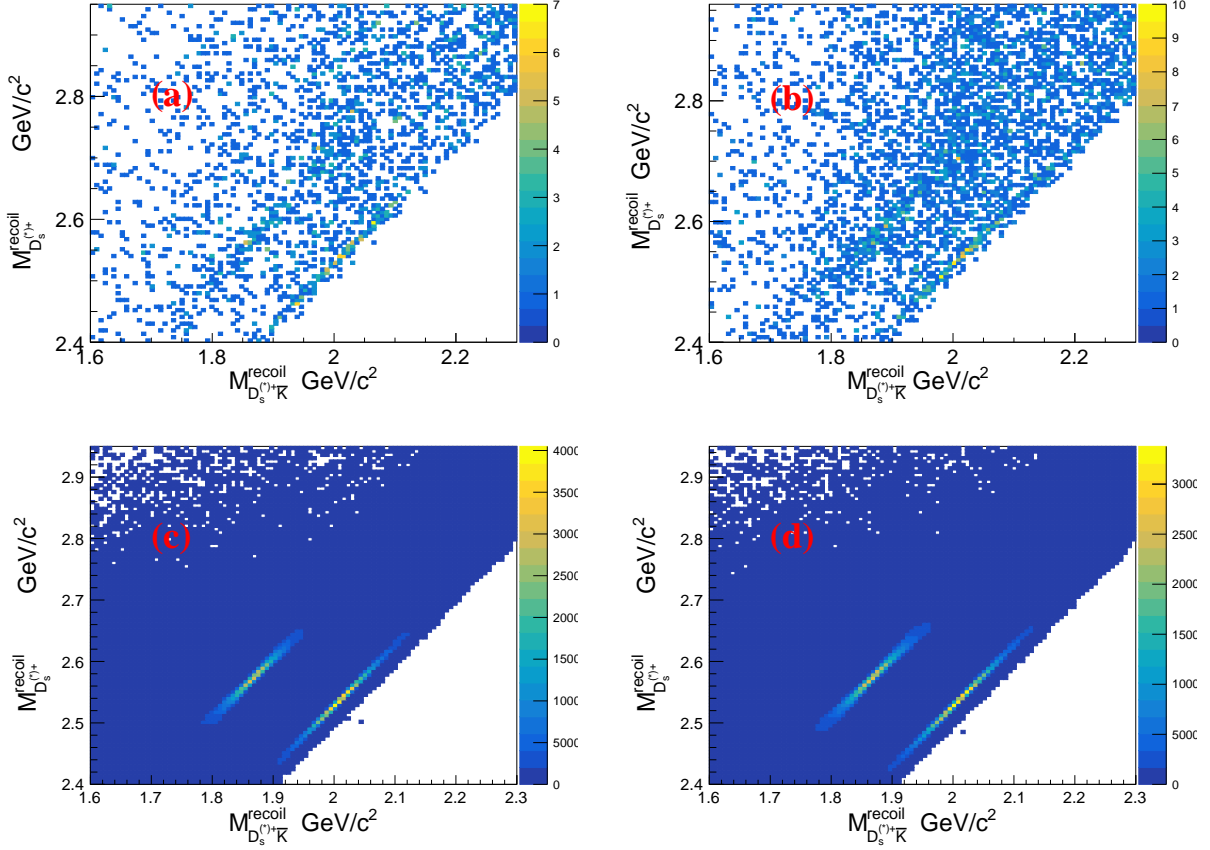


FIG. 2. The distributions of the recoil mass against $D_s^{(*)+} \bar{K}$ versus the recoil mass against $D_s^{(*)+}$ in (a) the $\Upsilon(2S)$ data sample, (b) the continuum data sample at $\sqrt{s} = 10.52$ GeV, (c) the signal MC simulation of $\Upsilon(2S)$ decays and (d) the signal MC simulation of continuum production at $\sqrt{s} = 10.52$ GeV.

To improve the mass resolution of $M_{\bar{K}\bar{D}^{(*)}}$, we use the following formula to replace Eq. (2):

$$M_{\bar{K}\bar{D}^{(*)}} = M_{D_s^{(*)+}}^{\text{recoil}} - M_{D_s^{(*)+} \bar{K}}^{\text{recoil}} + m_{\bar{D}^{(*)}}. \quad (3)$$

In this way, the uncertainties due to the 4-momentum of final states from $D_s^{(*)+}$ decays are significantly reduced. From simulation, we obtain the resolutions for $\Delta M^{\text{recoil}} \equiv M_{D_s^{(*)+}}^{\text{recoil}} - M_{D_s^{(*)+} \bar{K}}^{\text{recoil}}$ of $\sigma_{\Delta M^{\text{recoil}}} < 5$ MeV/ c^2 for all $D_s^{(*)+} D_{sJ}^-$ final states. In Figs. 3 and 4 we show the distributions for $\Delta M^{\text{recoil}} + m_{\bar{D}^*}$ for $M_{\bar{K}\bar{D}^*}$ and $\Delta M^{\text{recoil}} + m_{\bar{D}}$ for $M_{\bar{K}\bar{D}}$ for the two data samples. We observe clear signals for both $D_{s1}(2536)^-$ and $D_{s2}^*(2573)^-$.

We determine the numbers of D_{sJ}^- signals, $N_{\Upsilon(2S)}^{\text{sig}}$ of the $\Upsilon(2S)$ decays and $N_{\text{cont}}^{\text{sig}}$ of the continuum production at $\sqrt{s} = 10.52$ GeV, by simultaneously fitting the $M_{\bar{K}\bar{D}^{(*)}}$ distributions for the $\Upsilon(2S)$ data sample and the continuum data sample, and with common isospin ratios $R_{\text{iso},J} \equiv \mathcal{B}(D_{sJ}^- \rightarrow K_S^0 D^{(*)-}) / \mathcal{B}(D_{sJ}^- \rightarrow K^- \bar{D}^{(*)0})$ between the $K_S^0 D^{(*)-}$ and $K^- \bar{D}^{(*)0}$ final states. In the fits, we use $N_{\Upsilon(2S)}^{\text{sig}}$ and $N_{\text{cont}}^{\text{sig}}$ of the $K^- \bar{D}^{(*)0}$ modes, and those of the $K_S^0 D^{(*)-}$ modes are calculated via the isospin ratios $R_{\text{iso},J}$ and the ratios of efficiencies and branching fractions between the $K_S^0 D^{(*)-}$ modes and the $K^- \bar{D}^{(*)0}$ modes. The fit function

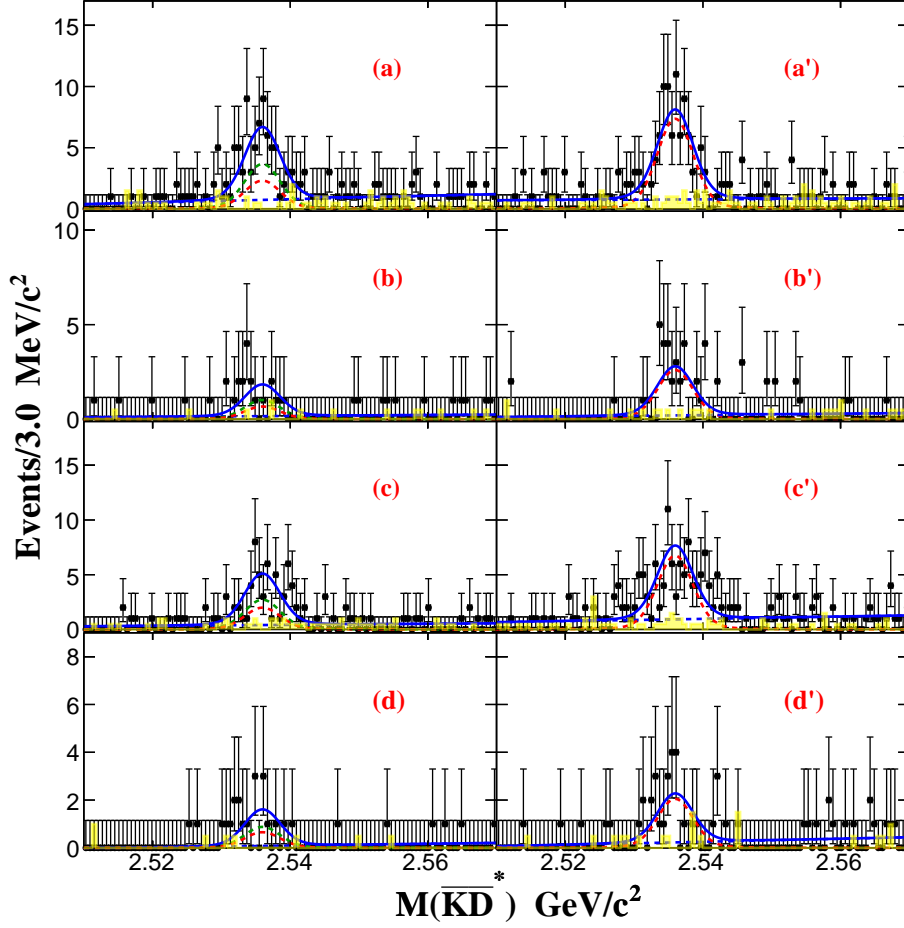


FIG. 3. The invariant mass distributions of $\bar{K}\bar{D}^*$ calculated in the recoil mass for $D_s^{(*)+}$ in the (a) $D_s^+ K^- \bar{D}^*(2007)^0$, (b) $D_s^+ K_S^0 D^*(2010)^-$, (c) $D_s^{*+} K^- \bar{D}^*(2007)^0$, and (d) $D_s^{*+} K_S^0 D^*(2010)^-$ final states from the $\Upsilon(2S)$ data sample (left panels) and the continuum data sample at 10.52 GeV (right panels). The shaded histograms show the backgrounds estimated from the normalized $D_s^{(*)+}$ mass sidebands. The solid curves show the best fit result; the dashed green ones are $D_{s1}(2536)^-$ signals in $\Upsilon(2S)$ decays and the dashed red curves are the $D_{s1}(2536)^-$ signals in continuum production at 10.02 GeV (left panels) and 10.52 GeV (right panels).

is the sum of a Breit-Wigner function (BW) convoluted with a Gaussian function with a width corresponding to the mass resolution, and a linear function to describe the backgrounds. The mass and width of the BW functions are fixed to the world average values for $D_{s1}(2536)^-$ and $D_{s2}^*(2573)^-$ [7]. The mass resolutions used in the Gaussian are obtained from MC simulations and are about 2.4 MeV/ c^2 (6.5 MeV/ c^2) for $D_{s1}(2536)^-$ ($D_{s2}^*(2573)^-$). In the fits, we include the branching fractions and reconstruction efficiencies corresponding to the $D_s^{(*)+} D_{sJ}^-$ final states. The results are listed in Table I for each channel and each data set.

We estimate the contribution of continuum production to the $D_s^{(*)+} D_{sJ}^-$ signal in the $\Upsilon(2S)$ data sample. For this, we scale the luminosities and correct for the c.m. energy dependence of the QED cross section $\sigma_{e^+e^-} \propto 1/s$, resulting in a scale factor $f_{\text{scale}} = (\mathcal{L}_{\Upsilon(2S)} \times s_{\text{cont}}) / (\mathcal{L}_{\text{cont}} \times s_{\Upsilon(2S)}) = 0.304$. Here, $\mathcal{L}_{\Upsilon(2S)}$ and $\mathcal{L}_{\text{cont}}$ are the integrated luminosities of the

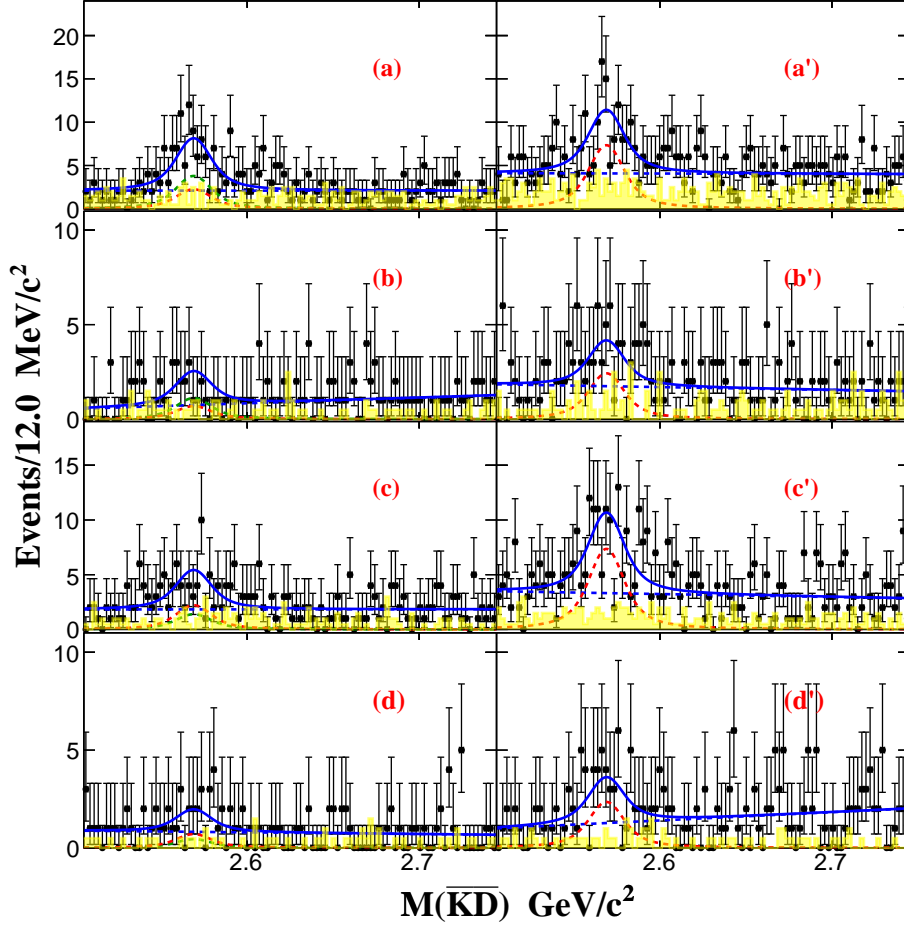


FIG. 4. The invariant mass distributions of $\bar{K}\bar{D}$ calculated in recoil mass for $D_s^{(*)+}$ in the (a) $D_s^+ K^- \bar{D}^0$, (b) $D_s^+ K_S^0 D^-$, (c) $D_s^{*+} K^- \bar{D}^0$, and (d) $D_s^{*+} K_S^0 D^-$ final states from the $\Upsilon(2S)$ data sample (left panels) and the continuum data sample at 10.52 GeV (right panels). The shaded histograms show the backgrounds estimated from the normalized $D_s^{(*)+}$ mass sidebands. The solid curves show the best fit result; the dashed green ones are $D_{s2}^{*}(2573)^-$ signals in $\Upsilon(2S)$ decays and the dashed red curves are the $D_{s2}^{*}(2573)^-$ signals in continuum production at 10.02 GeV (left panels) and 10.52 GeV (right panels).

$\Upsilon(2S)$ data sample at $\sqrt{s_{\Upsilon(2S)}} = 10.02$ GeV and the continuum data sample at $\sqrt{s_{\text{cont}}} = 10.52$ GeV. Therefore, the yield of signal events produced via continuum e^+e^- annihilation in the $\Upsilon(2S)$ data sample is $f_{\text{scale}} \times N_{\text{cont}}^{\text{sig}}$.

We determine the statistical significance of D_{sJ}^- by comparing the value of $\Delta(-2\ln L) = -2\ln(L_{\text{max}}/L_0)$ and the change in the number of free parameters in the fits, where L_{max} is the likelihood with D_{sJ}^- and L_0 without D_{sJ}^- . The statistical significance in the $\Upsilon(2S)$ data sample for $D_{s1}(2536)^-$ and $D_{s2}^{*}(2573)^-$ is 6.8σ and 4.0σ , respectively, and 18.3σ and 10.1σ in the continuum data sample. From these yields, we calculate the branching fraction of $\Upsilon(2S) \rightarrow D_s^{(*)+} D_{sJ}^-$ and the Born cross section for $e^+e^- \rightarrow D_s^{(*)+} D_{sJ}^+$ by

$$\mathcal{B}(\Upsilon(2S) \rightarrow D_s^{(*)+} D_{sJ}^-) \mathcal{B}(D_{sJ}^- \rightarrow \bar{K}\bar{D}^{(*)}) = \frac{N_{\Upsilon(2S)}^{\text{sig}}}{N_{\Upsilon(2S)} \times \sum \varepsilon_i \mathcal{B}_i}, \quad (4)$$

and

$$\sigma^B(e^+e^- \rightarrow D_s^{(*)+}D_{sJ}^-)\mathcal{B}(D_{sJ}^- \rightarrow \bar{K}\bar{D}^{(*)}) = \frac{N_{\text{cont}}^{\text{sig}} \times |1 - \Pi|^2}{\mathcal{L}_{\text{cont}} \times \sum \varepsilon_i \mathcal{B}_i \times (1 + \delta_{\text{ISR}})}. \quad (5)$$

Here, i identifies the mode of $D_s^+ \rightarrow h_1 h_2$ decay, while ε_i and \mathcal{B}_i are their reconstruction efficiencies and branching fractions. We calculate $\sum \varepsilon_i \mathcal{B}_i$ according to signal MC simulations for ε_i and the world average values of \mathcal{B}_i [7]. In the $D_s^{(*)+}D_{s1}(2536)^-$ channels, they are $(1.63 \pm 0.07)\%$, $(1.06 \pm 0.05)\%$, $(1.19 \pm 0.05)\%$, and $(0.77 \pm 0.03)\%$ in the final states of $D_s^+ K^- \bar{D}^*(2007)^0$, $D_s^+ K_S^0 D^*(2010)^-$, $D_s^{*+} K^- \bar{D}^*(2007)^0$, and $D_s^{*+} K_S^0 D^*(2010)^-$, respectively. In the $D_s^{(*)+}D_{s2}^*(2573)^-$ channels, they are $(2.32 \pm 0.10)\%$, $(1.56 \pm 0.07)\%$, $(1.22 \pm 0.05)\%$, and $(0.82 \pm 0.03)\%$ in the final states of $D_s^+ K^- \bar{D}^0$, $D_s^+ K_S^0 D^-$, $D_s^{*+} K^- \bar{D}^0$, and $D_s^{*+} K_S^0 D^-$, respectively. The errors of these values are mainly due to the uncertainties of \mathcal{B}_i from world averages [7], since all of the relative statistical uncertainties due to the statistics of MC simulations are less than 0.5%. Here, we take into account the branching fraction of $K_S^0 \rightarrow \pi^+ \pi^-$ decay [7]. From the Born cross-sections we can calculate the full “dressed” cross section through $\sigma^{\text{dressed}} = \sigma^{\text{Born}}/|1 - \Pi|^2$. The factor $|1 - \Pi|^2 = 0.931$ is the vacuum polarization factor [17, 18]. In addition, we have to correct for radiative effects. The radiative correction factor $1 + \delta_{\text{ISR}}$ is determined by $\int \sigma^{\text{dressed}}(s(1-x))F(x,s)dx/\sigma^{\text{dressed}}(s)$ and has the value 0.82, where $F(x,s)$ is the radiative function obtained from a QED calculation with an accuracy of 0.2% [19–21].

We summarize the branching fractions of $\Upsilon(2S)$ decays and the Born cross sections of continuum production in Table I. The number of corrected signal events in the $\Upsilon(2S)$ data sample is $20 \pm 12 \pm 2$ for the $D_s^{*+}D_{s2}^*(2573)^-$ decay, from which we derive a statistical significance of only 1.6σ . We integrate the likelihood versus the number of $D_s^{*+}D_{s2}^*(2573)^-$ signal events, and determine its upper limit at 90% confidence level (C.L.) to be $N^{\text{UL}}(\Upsilon(2S) \rightarrow D_s^{*+}D_{s2}^*(2573)^-) < 44$ in the $D_{s2}^*(2573)^- \rightarrow K^- \bar{D}^0$ mode, which has been degraded by a factor of $1/(1 - \delta_{\text{sys}})$ to account for the systematic uncertainties detailed below. We obtain an upper limit for the production in $\Upsilon(2S)$ decay of $\mathcal{B}^{\text{UL}}(\Upsilon(2S) \rightarrow D_s^{*+}D_{s2}^*(2573)^-)\mathcal{B}(D_{s2}^*(2573)^- \rightarrow K^- \bar{D}^0) < 2.5 \times 10^{-5}$.

Additionally, we determine the isospin ratios $R_{\text{iso},J}$ from the simultaneous fits to be $R_{\text{iso},1} = 0.48 \pm 0.07 \pm 0.02$ and $R_{\text{iso},2} = 0.49 \pm 0.10 \pm 0.02$ for the $D_{s1}(2536)^-$ and $D_{s2}^*(2573)^-$, respectively. These ratios are in good agreement with the expectation from isospin symmetry, which are 0.498 and 0.497 from a calculation taking into account the phase space. Replacing the $N_{\Upsilon(2S)}^{\text{sig}}$ and $N_{\text{cont}}^{\text{sig}}$ of $K^- \bar{D}^{(*)0}$ modes with those of the $K_S^0 D^{(*)-}$ modes in the simultaneous fits, and calculating those of the $K^- \bar{D}^{(*)0}$ modes with $R_{\text{iso},J}$ and the ratios of efficiencies and branching fractions between the $K^- \bar{D}^{(*)0}$ modes and the $K_S^0 D^{(*)-}$ modes, we obtain the new fit results and calculate the $\mathcal{B}(\Upsilon(2S) \rightarrow D_s^{(*)+}D_{sJ}^-)\mathcal{B}(D_{sJ}^- \rightarrow \bar{K}\bar{D}^{(*)})$ and $\sigma^B(e^+e^- \rightarrow D_s^{(*)+}D_{sJ}^-)\mathcal{B}(D_{sJ}^- \rightarrow \bar{K}\bar{D}^{(*)})$ of the $D_{sJ}^- \rightarrow K_S^0 D^{(*)-}$ decay modes, as listed in Table I. We get the same fit results of the isospin ratios $R_{\text{iso},J}$ of the $D_{s1}(2536)^-$ and $D_{s2}^*(2573)^-$ decays. We also determine the $N^{\text{UL}}(\Upsilon(2S) \rightarrow D_s^{*+}D_{s2}^*(2573)^-) < 15$ in the $K_S^0 D^-$ mode and $\mathcal{B}^{\text{UL}}(\Upsilon(2S) \rightarrow D_s^{*+}D_{s2}^*(2573)^-)\mathcal{B}(D_{s2}^*(2573)^- \rightarrow K_S^0 D^-) < 1.4 \times 10^{-5}$ at 90% C.L.

IV. SYSTEMATIC UNCERTAINTIES

The determination of the branching fractions in $\Upsilon(2S)$ decays and the Born cross sections of continuum productions are subject to a variety of systematic uncertainties, which are listed in Table II. The particle identification uncertainty for K^\pm is 1.1% and 0.9% per

TABLE I. The branching fractions of $\Upsilon(2S) \rightarrow D_s^{(*)+} D_{sJ}^-$ decays and the Born cross sections of continuum production $e^+e^- \rightarrow D_s^{(*)+} D_{sJ}^-$ based on the results from the simultaneous fits. Here, $N_{\Upsilon(2S)}^{\text{sig}}$, $N_{\text{cont}}^{\text{sig}}$, $\mathcal{B}(\Upsilon(2S) \rightarrow D_s^{(*)+} D_{sJ}^-) \mathcal{B}(D_{sJ}^- \rightarrow \bar{K} \bar{D}^{(*)})$, and $\sigma^{\text{B}}(e^+e^- \rightarrow D_s^{(*)+} D_{sJ}^-) \mathcal{B}(D_{sJ}^- \rightarrow \bar{K} \bar{D}^{(*)})$ are described in Eqs. (4) and (5). The significance is the statistical significance of the $D_s^{(*)+} D_{sJ}^-$ signals with $D_{sJ}^- \rightarrow K^- D^{(*)0}$ and $K_S^0 D^{(*)-}$ in $\Upsilon(2S)$ decays and continuum productions. The $K^- D^{(*)0}$ and $K_S^0 D^{(*)-}$ modes of the D_{sJ}^- decays are connected by the isospin ratio $\mathcal{B}(D_{sJ}^- \rightarrow K^- \bar{D}^{(*)0}) / \mathcal{B}(D_{sJ}^- \rightarrow K^- \bar{D}^{(*)0})$ in the simultaneous fits. The systematic uncertainties of N^{sig} are of the simultaneous fits only.

Final state (f)	$N_{\Upsilon(2S)}^{\text{sig}}$		Significance (σ)	$\mathcal{B}(\Upsilon(2S) \rightarrow D_s^{(*)+} D_{sJ}^-) \mathcal{B}(D_{sJ}^- \rightarrow \bar{K} \bar{D}^{(*)})$	
	K^- mode	K_S^0 mode		K^- mode	K_S^0 mode
$D_s^+ D_{s1}(2536)^-$	$43 \pm 9 \pm 2$	$14 \pm 3 \pm 2$	5.3	$1.6 \pm 0.3 \pm 0.2$	$0.84 \pm 0.18 \pm 0.14$
$D_s^{*+} D_{s1}(2536)^-$	$31 \pm 8 \pm 2$	$10 \pm 3 \pm 2$	4.3	$1.4 \pm 0.4 \pm 0.2$	$0.82 \pm 0.25 \pm 0.18$
$D_s^+ D_{s2}^*(2573)^-$	$51 \pm 15 \pm 5$	$17 \pm 5 \pm 5$	3.8	$1.4 \pm 0.4 \pm 0.2$	$0.69 \pm 0.20 \pm 0.21$
$D_s^{*+} D_{s2}^*(2573)^-$	$20 \pm 12 \pm 2$	$7 \pm 4 \pm 4$	1.6	$0.9 \pm 0.5 \pm 0.1$	$0.54 \pm 0.31 \pm 0.39$
—	$N_{\text{cont}}^{\text{sig}}$		—	$\sigma^{\text{B}}(e^+e^- \rightarrow D_s^{(*)+} D_{sJ}^-) \mathcal{B}(D_{sJ}^- \rightarrow \bar{K} \bar{D}^{(*)})$	
	K^- mode	K_S^0 mode		K^- mode	K_S^0 mode
$D_s^+ D_{s1}(2536)^-$	$86 \pm 10 \pm 2$	$28 \pm 4 \pm 2$	13.9	$67 \pm 8 \pm 6$	$34 \pm 5 \pm 4$
$D_s^{*+} D_{s1}(2536)^-$	$79 \pm 10 \pm 2$	$25 \pm 4 \pm 2$	11.8	$84 \pm 11 \pm 11$	$41 \pm 6 \pm 6$
$D_s^+ D_{s2}^*(2573)^-$	$102 \pm 17 \pm 21$	$33 \pm 8 \pm 5$	7.1	$56 \pm 9 \pm 13$	$27 \pm 6 \pm 5$
$D_s^{*+} D_{s2}^*(2573)^-$	$102 \pm 16 \pm 6$	$33 \pm 7 \pm 4$	7.6	$106 \pm 17 \pm 12$	$51 \pm 11 \pm 9$
Isospin ratio $\mathcal{B}(D_{sJ}^- \rightarrow K_S^0 D^{(*)-}) / \mathcal{B}(D_{sJ}^- \rightarrow K^- \bar{D}^{(*)0})$					
$D_{s1}(2536)^-$ decays			$0.48 \pm 0.07 \pm 0.02$		
$D_{s2}^*(2573)^-$ decays			$0.49 \pm 0.10 \pm 0.02$		

π^\pm [14]; the uncertainty of the tracking efficiency per track is 0.35% and is added linearly; the photon reconstruction uncertainty is 2% for each photon. The uncertainties of the efficiency of mass window requirements due to data and MC differences in mass resolutions for π^0 , K_S^0 , $\bar{K}^*(892)^0$, ρ^+ , ϕ , η , and η' are measured to be 0.2%, 0.2%, 1.0%, 1.4%, 0.1%, 1.7%, and 0.3%, respectively. We take the decay branching fractions and their uncertainties of the intermediate states $\bar{K}^*(892)^0$, η , ρ^+ , η' , and of $D_s^{(*)+}$ from Ref. [7]. We determine the efficiency of the D_s^+ (D_s^{*+}) mass window to be $(99.9 \pm 0.1)\%$ $[(99.8 \pm 0.1)\%]$ in data and 97.4% (99.5%) in the simulation, and we attribute a systematic uncertainty of 2.5% (0.3%); the differences in these numbers for data and simulation reflect the different mass resolutions obtained for both. We determine these total uncertainties of $\sum \varepsilon_i \times \mathcal{B}_i$ to be 3.2%, 3.2%, 3.3%, and 3.4% in the final states of $D_s^+ K^- \bar{D}^{(*)0}$, $D_s^+ K_S^0 D^{(*)-}$, $D_s^{*+} K^- \bar{D}^{(*)0}$, and $D_s^{*+} K_S^0 D^{(*)-}$, respectively. To estimate the systematic uncertainty in the angular distribution of $D_s^{(*)+} D_{sJ}^-$, we generate new MC samples uniformly in phase space, and half of the efficiency differences are taken to be the systematic uncertainties. We get the systematic uncertainties of 6.9%, 8.5%, 8.5%, and 9.2% for the $D_s^+ D_{s1}(2536)^-$, $D_s^+ D_{s2}^*(2573)^-$, $D_s^{*+} D_{s1}(2536)^-$, and $D_s^{*+} D_{s2}^*(2573)^-$, respectively. The uncertainty of the total number of $\Upsilon(2S)$ events is 2.2%. The uncertainty in

the integrated luminosities for the two data samples are 1.4% and are highly correlated, but they cancel in the scale factor. We estimate the systematic uncertainty in determining the $\mathcal{B}^{\text{UL}}(\Upsilon(2S) \rightarrow D_s^{*+} D_{s2}^*(2573)^-)\mathcal{B}(D_{s2}^*(2573)^- \rightarrow K^- \bar{D}^0)$ to be $\delta_{\text{sys}} = 10.1\%$. Besides those listed in Table II, there are additional systematic uncertainties of the scale factor f_{scale} and the radiative correction factor $1 + \delta_{\text{ISR}}$. By changing $s_{\text{cont}}/s_{\Upsilon(2S)}$ to $[s_{\text{cont}}/s_{\Upsilon(2S)}]^{1.5}$, the value of f_{scale} changes from 0.304 to 0.319, and we take 4.9% to be its systematic uncertainty. By varying the photon energy cutoff 50 MeV in the simulation of ISR, we determine the change of $1 + \delta_{\text{ISR}}$ to be 0.01 and take 1.0% to be the conservative systematic uncertainty.

Various systematic uncertainties are considered in the simultaneous fit. We change the fit range from $[2.51, 2.57]$ GeV/ c^2 to $[2.51, 2.62]$ GeV/ c^2 for the $D_{s1}(2536)^-$ signals, and from $[2.50, 2.74]$ GeV/ c^2 to $[2.50, 2.79]$ GeV/ c^2 for the $D_{s2}^*(2573)^-$ signals. We vary the mass and width of $D_{s1}(2536)^-$ or $D_{s2}^*(2573)^-$ by 1σ according to the world average values [7]. We also change the mass resolutions from the signal MC simulations by 1σ , and the systematic uncertainties are found to be negligible.

V. SUMMARY

In summary, we observe the charmed strange meson pair $D_s^{(*)+} D_{sJ}^-$ production in $\Upsilon(2S)$ decays and in e^+e^- annihilation at $\sqrt{s} = 10.52$ GeV for the first time, where D_{sJ}^- is $D_{s1}(2536)^-$ or $D_{s2}^*(2573)^-$. We determine the products of branching fractions for the D_{sJ}^- production in $\Upsilon(2S)$ decays to be

$$\begin{aligned}\mathcal{B}(\Upsilon(2S) \rightarrow D_s^+ D_{s1}(2536)^-)\mathcal{B}(D_{s1}(2536)^- \rightarrow K^- D^*(2007)^0) &= (1.6 \pm 0.3 \pm 0.2) \times 10^{-5}, \\ \mathcal{B}(\Upsilon(2S) \rightarrow D_s^{*+} D_{s1}(2536)^-)\mathcal{B}(D_{s1}(2536)^- \rightarrow K^- D^*(2007)^0) &= (1.4 \pm 0.4 \pm 0.2) \times 10^{-5}, \\ \mathcal{B}(\Upsilon(2S) \rightarrow D_s^+ D_{s2}^*(2573)^-)\mathcal{B}(D_{s2}^*(2573)^- \rightarrow K^- D^0) &= (1.4 \pm 0.4 \pm 0.2) \times 10^{-5}, \\ \mathcal{B}(\Upsilon(2S) \rightarrow D_s^{*+} D_{s2}^*(2573)^-)\mathcal{B}(D_{s2}^*(2573)^- \rightarrow K^- D^0) &= (0.9 \pm 0.5 \pm 0.1) \times 10^{-5},\end{aligned}$$

and

$$\begin{aligned}\mathcal{B}(\Upsilon(2S) \rightarrow D_s^+ D_{s1}(2536)^-)\mathcal{B}(D_{s1}(2536)^- \rightarrow K_S^0 D^*(2010)^-) &= (0.84 \pm 0.18 \pm 0.14) \times 10^{-5}, \\ \mathcal{B}(\Upsilon(2S) \rightarrow D_s^{*+} D_{s1}(2536)^-)\mathcal{B}(D_{s1}(2536)^- \rightarrow K_S^0 D^*(2010)^-) &= (0.82 \pm 0.25 \pm 0.18) \times 10^{-5}, \\ \mathcal{B}(\Upsilon(2S) \rightarrow D_s^+ D_{s2}^*(2573)^-)\mathcal{B}(D_{s2}^*(2573)^- \rightarrow K_S^0 D^-) &= (0.69 \pm 0.20 \pm 0.21) \times 10^{-5}, \\ \mathcal{B}(\Upsilon(2S) \rightarrow D_s^{*+} D_{s2}^*(2573)^-)\mathcal{B}(D_{s2}^*(2573)^- \rightarrow K_S^0 D^-) &= (0.54 \pm 0.31 \pm 0.39) \times 10^{-5}.\end{aligned}$$

We also determine the upper limit $\mathcal{B}^{\text{UL}}(\Upsilon(2S) \rightarrow D_s^{*+} D_{s2}^*(2573)^-)\mathcal{B}(D_{s2}^*(2573)^- \rightarrow K^- \bar{D}^0) < 2.5 \times 10^{-5}$ and $\mathcal{B}^{\text{UL}}(\Upsilon(2S) \rightarrow D_s^{*+} D_{s2}^*(2573)^-)\mathcal{B}(D_{s2}^*(2573)^- \rightarrow K_S^0 D^-) < 1.4 \times 10^{-5}$ at 90% C.L. We determine Born cross sections for continuum productions of the D_{sJ}^- at $\sqrt{s} = 10.52$ GeV to be

$$\begin{aligned}\sigma^{\text{Born}}(e^+e^- \rightarrow D_s^+ D_{s1}(2536)^-)\mathcal{B}(D_{s1}(2536)^- \rightarrow K^- D^*(2007)^0) &= (67 \pm 8 \pm 6) \text{ fb}, \\ \sigma^{\text{Born}}(e^+e^- \rightarrow D_s^{*+} D_{s1}(2536)^-)\mathcal{B}(D_{s1}(2536)^- \rightarrow K^- D^*(2007)^0) &= (84 \pm 11 \pm 11) \text{ fb}, \\ \sigma^{\text{Born}}(e^+e^- \rightarrow D_s^+ D_{s2}^*(2573)^-)\mathcal{B}(D_{s2}^*(2573)^- \rightarrow K^- D^0) &= (56 \pm 9 \pm 13) \text{ fb}, \\ \sigma^{\text{Born}}(e^+e^- \rightarrow D_s^{*+} D_{s2}^*(2573)^-)\mathcal{B}(D_{s2}^*(2573)^- \rightarrow K^- D^0) &= (106 \pm 17 \pm 12) \text{ fb},\end{aligned}$$

and

$$\sigma^{\text{Born}}(e^+e^- \rightarrow D_s^+ D_{s1}(2536)^-)\mathcal{B}(D_{s1}(2536)^- \rightarrow K_S^0 D^*(2010)^-) = (34 \pm 5 \pm 4) \text{ fb},$$

TABLE II. The summary of systematic uncertainties (%) of $D_s^{(*)+} K$ reconstruction.

		D_s^+ reconstruction								
D_s^+ decay mode		$\phi\pi^+$	$K_S^0 K^+$	$\bar{K}^{*+}(892) K^+$	$\rho^+ \phi$	$\eta\pi^+(\gamma\gamma/\pi^+\pi^-\pi^0)$	$\eta'\pi^+(\gamma\gamma/\pi^+\pi^-\pi^0)$	K^-	K_S^0	
Source	K ID	2.20	1.10	2.20	2.20	—	—	1.10	—	
	π ID	0.90	—	0.90	0.90	0.90/2.70	2.70/4.50	—	—	
	Tracking	1.05	1.05	1.05	1.05	0.35/1.05	1.05/1.75	0.35	—	
	K_S^0 reconstruction	—	2.23	—	—	—	—	—	2.23	
	π^0 reconstruction	—	—	—	2.25	2.25/—	2.25/—	—	—	
	Photon reconstruction	—	—	—	—	4.0/—	4.0/—	—	—	
	Mass windows of intermediate states	0.07	0.20	0.97	1.44	0.23/1.68	0.26/1.69	—	0.20	
	\mathcal{B} s of intermediate state decays	0.08	0.08	0.08	1.12	0.04/0.03	0.04/0.03	—	—	
	D_s^+ mass window	0.43	0.67	0.19	0.79	1.07	1.20	—	—	
	D_s^{*+} mass window	0.38	1.01	0.10	0.34	0.94	0.61	—	—	
Reconstruction mode		$D_s^+ K^-$	$D_s^+ K_S^0$	$D_s^{*+} K^-$					$D_s^{*+} K_S^0$	
Source	$D_s^{(*)+} K$ reconstruction	3.2	3.2	3.3					3.4	
	$\mathcal{B}(D_s^{*+} \rightarrow \gamma D_s^+)$	—	—	0.7					0.7	
	Trigger	1.0	1.0	1.0					1.0	
	MC statistics	0.2	0.2	0.2					0.2	
	$N_{\Upsilon(2S)}$ (luminosity)	2.2(1.4)	2.2(1.4)	2.2(1.4)					2.2(1.4)	
	Sum in quadrature	4.0(3.6)	4.0(3.6)	4.2(3.8)					4.2(3.9)	

Additional uncertainties due to the angular distributions are 6.9%, 8.5%, 8.5%, and 9.2% for the $D_s^+ D_{s1}(2536)^-$, $D_s^+ D_{s2}^*(2573)^-$, $D_s^{*+} D_{s1}(2536)^-$, and $D_s^{*+} D_{s2}^*(2573)^-$, respectively.

$$\begin{aligned}
\sigma^{\text{Born}}(e^+e^- \rightarrow D_s^{*+}D_{s1}(2536)^-)\mathcal{B}(D_{s1}(2536)^- \rightarrow K_S^0D^*(2010)^-) &= (41 \pm 6 \pm 6) \text{ fb}, \\
\sigma^{\text{Born}}(e^+e^- \rightarrow D_s^+D_{s2}^*(2573)^-)\mathcal{B}(D_{s2}^*(2573)^- \rightarrow K_S^0D^-) &= (27 \pm 6 \pm 5) \text{ fb}, \\
\sigma^{\text{Born}}(e^+e^- \rightarrow D_s^{*+}D_{s2}^*(2573)^-)\mathcal{B}(D_{s2}^*(2573)^- \rightarrow K_S^0D^-) &= (51 \pm 11 \pm 9) \text{ fb},
\end{aligned}$$

For comparison, $\sigma^{\text{Born}}(e^+e^- \rightarrow \mu^+\mu^-) = 0.784 \text{ nb}$ at $\sqrt{s} = 10.52 \text{ GeV}$ and $\mathcal{B}(\Upsilon(2S) \rightarrow \mu^+\mu^-) = (1.93 \pm 0.17)\%$ [7]. We define the ratios $R_1 \equiv \mathcal{B}(\Upsilon(2S) \rightarrow D_s^{(*)+}D_{sJ}^-)/\mathcal{B}(\Upsilon(2S) \rightarrow \mu^+\mu^-)$ for the $\Upsilon(2S)$ decays and $R_2 \equiv \sigma^{\text{Born}}(e^+e^- \rightarrow D_s^{(*)+}D_{sJ}^-)/\sigma^{\text{Born}}(e^+e^- \rightarrow \mu^+\mu^-)$ for the continuum productions. We obtain $R_1/R_2 = 9.7 \pm 2.3 \pm 1.1$, $6.8 \pm 2.1 \pm 0.8$, $10.2 \pm 3.3 \pm 2.5$, and $3.4 \pm 2.1 \pm 0.5$ for the $D_s^+D_{s1}(2536)^-$, $D_s^{*+}D_{s1}(2536)^-$, $D_s^+D_{s2}^*(2573)^-$, and $D_s^{*+}D_{s2}^*(2573)^-$ final states in the $D_{sJ}^- \rightarrow K^-\bar{D}^{(*)0}$ modes, respectively, where the uncertainty of $\mathcal{B}(\Upsilon(2S) \rightarrow \mu^+\mu^-)$ is taken into account of the systematic uncertainties. Therefore, the strong decay is expected to dominate in $\Upsilon(2S) \rightarrow D_s^{(*)+}D_{sJ}^-$ processes.

Here, we also determine the ratios of branching fractions to be

$$\begin{aligned}
\mathcal{B}(D_{s1}(2536)^- \rightarrow K_S^0D^*(2010)^-)/\mathcal{B}(D_{s1}(2536)^- \rightarrow K^-D^*(2007)^0) &= 0.48 \pm 0.07 \pm 0.02, \\
\mathcal{B}(D_{s2}^*(2573)^- \rightarrow K_S^0D^-)/\mathcal{B}(D_{s2}^*(2573)^- \rightarrow K^-D^0) &= 0.49 \pm 0.10 \pm 0.02,
\end{aligned}$$

which are in good agreement with the expected 0.498 and 0.497 from isospin symmetry considering the phase space, since with K_S^0 only half of the neutral kaons can be reconstructed. The first ratio has same precision in comparison to the world average value [7], while the second ratio is the first measurement of this quantity.

ACKNOWLEDGMENTS

This work, based on data collected using the Belle detector, which was operated until June 2010, was supported by the Ministry of Education, Culture, Sports, Science, and Technology (MEXT) of Japan, the Japan Society for the Promotion of Science (JSPS), and the Tau-Lepton Physics Research Center of Nagoya University; the Australian Research Council including grants DP210101900, DP210102831, DE220100462, LE210100098, LE230100085; Austrian Federal Ministry of Education, Science and Research (FWF) and FWF Austrian Science Fund No. P 31361-N36; National Key R&D Program of China under Contract No. 2022YFA1601903, National Natural Science Foundation of China and research grants No. 11575017, No. 11761141009, No. 11705209, No. 11975076, No. 12135005, No. 12150004, No. 12161141008, and No. 12175041, and Shandong Provincial Natural Science Foundation Project ZR2022JQ02; the Ministry of Education, Youth and Sports of the Czech Republic under Contract No. LTT17020; the Czech Science Foundation Grant No. 22-18469S; Horizon 2020 ERC Advanced Grant No. 884719 and ERC Starting Grant No. 947006 “InterLeptons” (European Union); the Carl Zeiss Foundation, the Deutsche Forschungsgemeinschaft, the Excellence Cluster Universe, and the VolkswagenStiftung; the Department of Atomic Energy (Project Identification No. RTI 4002) and the Department of Science and Technology of India; the Istituto Nazionale di Fisica Nucleare of Italy; National Research Foundation (NRF) of Korea Grant Nos. 2016R1D1A1B02012900, 2018R1A2B3003643, 2018R1A6A1A-06024970, RS202200197659, 2019R1I1A3A01058933, 2021R1A6A1A03043957, 2021R1F1A-1060423, 2021R1F1A1064008, 2022R1A2C1003993; Radiation Science Research Institute, Foreign Large-size Research Facility Application Supporting project, the Global Science Experimental Data Hub Center of the Korea Institute of Science and Technology Information and KREONET/GLORIAD; the Polish Ministry of Science and Higher Education and

the National Science Center; the Ministry of Science and Higher Education of the Russian Federation, Agreement 14.W03.31.0026, and the HSE University Basic Research Program, Moscow; University of Tabuk research grants S-1440-0321, S-0256-1438, and S-0280-1439 (Saudi Arabia); the Slovenian Research Agency Grant Nos. J1-9124 and P1-0135; Ikerbasque, Basque Foundation for Science, Spain; the Swiss National Science Foundation; the Ministry of Education and the Ministry of Science and Technology of Taiwan; and the United States Department of Energy and the National Science Foundation. These acknowledgements are not to be interpreted as an endorsement of any statement made by any of our institutes, funding agencies, governments, or their representatives. We thank the KEKB group for the excellent operation of the accelerator; the KEK cryogenics group for the efficient operation of the solenoid; and the KEK computer group and the Pacific Northwest National Laboratory (PNNL) Environmental Molecular Sciences Laboratory (EMSL) computing group for strong computing support; and the National Institute of Informatics, and Science Information NETwork 6 (SINET6) for valuable network support.

-
- [1] N. Brambilla *et al.*, Phys. Rep. **873** (2020) 1.
 - [2] N. Brambilla *et al.*, Eur. Phys. J. C **71** (2011) 1534.
 - [3] H. Fritzsche and K. H. Streng, Phys. Lett. B **77** (1978) 299.
 - [4] B. Aubert *et al.* (BaBar Collaboration), Phys. Rev. D **81** (2010) 011102.
 - [5] D. Kang, T. Kim, J. Lee, and C. Yu, Phys. Rev. D **76** (2007) 114018.
 - [6] Y. J. Zhang and K. T. Chao, Phys. Rev. D **78** (2008) 094017.
 - [7] R. L. Workman *et al.* (Particle Data Group), Prog. Theor. Exp. Phys. **2022** (2022) 083C01.
 - [8] I. I. Y. Bigi and S. Nussinov, Phys. Lett. B **82** (1979) 281.
 - [9] S. Kurokawa and E. Kikutani, Nucl. Instrum. Meth. A **499** (2003) 1, and other papers included in this Volume; T. Abe *et al.*, Prog. Theor. Exp. Phys. **2013** (2013) 03A001 and references therein. S. Kurokawa and E. Kikutani, Nucl. Instrum. Meth. A **499** (2003) 1, and other papers included in this volume.
 - [10] A. Abashian *et al.* (Belle Collaboration), Nucl. Instrum. Meth. A **479** (2002) 117; also see detector section in J. Brodzicka *et al.*, Prog. Theor. Exp. Phys. **2012** (2012) 04D001.
 - [11] D. J. Lange, Nucl. Instrum. Meth. A **462** (2001) 152.
 - [12] M. Ablikim *et al.* (BESIII Collaboration), arXiv:2305.14631v1.
 - [13] R. Brun *et al.*, GEANT 3.21, CERN Report DD/EE/84-1 (1984).
 - [14] E. Nakano, Nucl. Instrum. Meth. A **494** (2002) 402.
 - [15] H. Nakano, Ph.D. thesis, Tohoku University, 2014.
 - [16] M. Feindt and U. Kerzel, Nucl. Instrum. Meth. A **599** (2006) 190.
 - [17] S. Actis *et al.*, Eur. Phys. J. C **66** (2010) 585.
 - [18] X. K. Dong, X. H. Mo, P. Wang, and C. Z. Yuan, Chin. Phys. C **44** (2020) 083001.
 - [19] E. A. Kuraev and V. S. Fadin, Yad. Fiz. **41**, 733(1985) [Sov. J. Nucl. Phys. **41**, 466(1985)].
 - [20] S. Jadach, B. F. L. Ward, and Z. Was, Phys. Rev. D **63** (2001) 113009; Comput. Phys. Commun. **130**, 260(2000).
 - [21] M. Benayoun, S. I. Eidelman, V. N. Ivanchenko, and Z. K. Silagadze, Mod. Phys. Lett. A **14**, 2605(1999).